Journal of Hazardous Materials 183 (2010) 554–564

Contents lists available at ScienceDirect

Journal of Hazardous Materials

journal homepage: www.elsevier.com/locate/jhazmat

Synthesis of hybrid silica materials with tunable pore structures and morphology and their application for heavy metal removal from drinking water

Kaisheng Xia [a], Richard Z. Ferguson [a,b], Manon Losier [b], Nadéjda Tchoukanova [b], Ralf Brüning [c], Yahia Djaoued [a,*]

[a] Laboratoire de Micro-spectroscopies Raman et FTIR, Université de Moncton – Campus de Shippagan, Shippagan, NB E8S 1P6, Canada
[b] Institut de Recherche sur les Zones Côtières Inc., Volet Laboratoires & Services d'Analyses, Shippagan, NB E8S 1J2, Canada
[c] Physics Department, Mount Allison University, Sackville, NB E4L 1E4, Canada

ARTICLE INFO

Article history:
Received 26 April 2010
Received in revised form 9 July 2010
Accepted 13 July 2010
Available online 21 July 2010

Keywords:
Porous silica
Organic–inorganic hybrid
Heavy metals
Adsorption

ABSTRACT

Porous silica materials S8, S12, S16, and SBA with controllable pore structures and morphology were synthesized by varying the type or alkyl chain length of the surfactant. Diverse amino-functionalized organic–inorganic hybrid porous materials were then prepared by post-grafting. Depending on the relation between the pore diameter of the porous silica materials and the size and content of the moiety to be grafted, the functionalized materials exhibited varying degrees of decline of structure properties, i.e. regular arrangement of pores, specific surface area, pore size, and pore volume. The hybrid silica materials have been employed as heavy metal ions adsorbents from simulated drinking water at room temperature. The results indicated that the diverse pore structures and different amino group densities influence the heavy metal ions adsorption of functionalized silicas significantly. The best adsorbent was found to be monoamino-functionalized silica S16-1N, which could effectively remove heavy metal Cd(II), Pb(II), Fe(III), as well as Mn(II). The good performance can be attributed to the accessibility of effective amino groups in the pores, as well as the suitable pore structure with high specific surface area of 728 m^2/g and total pore volume of 0.34 cm^3/g.

1. Introduction

A wide variety of toxic substances have been directly discharged to the environment as industrial wastes, causing serious water, air, and soil pollution. Many heavy metals such as Cd(II), Cu(II), Pb(II), Hg(II), and Zn(II) are found in wastewater streams stemming from chemical manufacturing, electrical apparatus, painting and coating, pigments, mining, battery, nuclear, and other industries [1]. The toxic metals threaten the aquatic ecosystem and the human health. In recent years, the removal of heavy metals from aqueous solutions has been one of the major problems on wastewater treatment. Many techniques can be used to remove the heavy metals, such as chemical precipitation, ion-exchange, adsorption, and reverse osmosis. Among the available methods, adsorption technology has attracted attention due to its simplicity and low cost. Activated carbon, coal fly ash and zeolite have been used for the removal of heavy metal ions [2–6]. Some adsorbents have been proved to have good adsorption capacity. However, in some cases these adsorbents have poor removal efficiencies for low concentrations of metal ions. Moreover, their relatively weak interaction with metal ions leads to considerable leaching [7]. To overcome this drawback, hybrid organic–inorganic mesoporous silicas have been lately proposed as heavy metal adsorbents. These silica-based adsorbents have unique large specific surface areas, regular pore structures, and a high density of adsorption sites. The functional groups on the pore surface of adsorbents can effectively trap metallic cations. Moreover, they are adaptable to environment and can also be regenerated for many times after adsorption saturation.

Since the pioneering work of Feng et al. [8] and Mercier and Pinnavaia [9] in 1997, a lot of works have been carried out regarding hybrid mesoporous silicas for removal of heavy metals over the past decade [10–23]. These hybrid materials have shown promise as a remedy for polluted waters. Mesoporous silicas are usually modified by functional groups (–NH_2, –SH, –S–, etc.) to afford these materials the ability to interact strongly with metallic cations. There are two independent methods to introduce functional groups into a mesoporous matrix, namely post-grafting and co-condensation. The numerous silanol groups at the pore surfaces of mesoporous silicas can anchor large amounts of silanes and thus the functional groups are introduced into the mesoporous silicas. These abundant adsorption sites have a spectrum of binding ener-

* Corresponding author at: Laboratoire de Micro-spectroscopies Raman et FTIR, Université de Moncton – Campus de Shippagan, 218, Boul. J.-D. Gauthier, Shippagan, NB E8S 1P6, Canada. Tel.: +1 506 336 3412; fax: +1 506 336 3434.
E-mail address: djaoued@umcs.ca (Y. Djaoued).

0304-3894/$ – see front matter © 2010 Elsevier B.V. All rights reserved.
doi:10.1016/j.jhazmat.2010.07.060

gies. According to the HSAB (Hard and Soft Acids and Bases) theory [24], the adsorption is achieved through the strong affinity of the functional groups for metallic cations and the formation of strong chemical bonds between them.

Numerous works indicate that the adsorption capacity of the hybrid mesoporous silicas is related to both the surface density of the functional groups and their porous framework structure. Most of the previous work has been concerned with well-known mesoporous silicas such as MCM-41 [8,11,15,16], SBA-15 [10,16,17,22], and SBA-1, HMS, or FDU [9,11,14,19], and investigations of less common mesoporous silicas are rare. In this work, porous silica materials were synthesized using a modified cationic surfactant method [25,26]. The addition of a short chain alcohol as a co-solvent allows control of the morphology during the synthesis. In order to clarify the effect of the different pore structures of mesoporous silicas on heavy metal removal, silicas with different pore diameters were prepared by varying the carbon chain length of alkyltrimethylammonium bromide. For comparison, SBA-type mesoporous silica was also synthesized. The functional amino groups have been proved to be excellent in chelating many kinds of heavy metals and can thus enhance the adsorption capability of the adsorbents [11]. Meanwhile, a recent study showed that post-grafting functionalization is superior to co-condensation for obtaining a large number of accessible amino groups [27]. Thus, monoamino, diamino and triamino ligands were grafted on the pore surface of varied silicas to form hybrid organic–inorganic nanoporous silica adsorbents. These diverse and peculiar hybrid silicas were tested as heavy metal removal materials in drinking water treatment. We explored the influence of the diverse pore structures and the different amino group densities on heavy metal removal.

2. Experimental

2.1. Synthesis of mesoporous silicas

The mesoporous silicas with different pore diameters were prepared using the nonionic triblock copolymer surfactant $EO_{20}PO_{70}EO_{20}$ (Pluronic P123, BASF), or the cationic surfactant alkyltrimethylammonium bromide C_nTMABr (n = 8, 12, 16) (Aldrich) as template and tetraethyl orthosilicate (TEOS, Aldrich) as the silica source. The silica SBA was obtained using P123 as the surfactant in acid media according to a published procedure [28]. In the synthesis of SBA, the crystallization of silica gel was carried out via a hydrothermal treatment at 90 °C for 24 h. The structure-directed assembly of SBA involves a combination of electrostatic and hydrogen-bonding interactions. Under acidic conditions, the PPO block is expected to display more hydrophobicity than the PEO block upon heating. At pH ≈ 1, positively charged protonated silicate species interact preferentially with the more hydrophilic PEO block or blocks to promote cooperative self-assembly of a silica-block-polymer-rich mesophase from a dilute water-rich phase. Concurrent and further condensation of the silica species in the presence of Pluronic P123 results in the formation of the hexagonal mesophase silica composite. Silicas were synthesized using alkyltrimethylammonium bromide with different lengths of alkyl chains according to the following procedure. First, 6.15 g of octyltrimethylammonium bromide ($C_8H_{17}(CH_3)_3NBr$), 5.20 g of dodecyltrimethylammonium bromide ($C_{12}H_{25}(CH_3)_3NBr$), or 6.15 g of hexadecyltrimethylammonium bromide ($C_{16}H_{33}(CH_3)_3NBr$) was dissolved in a mixture of 284 mL of distilled water and 118 mL of ethanol. Under continuous stirring, 28.4 mL of ammonia solution (28–30 wt.%, Aldrich) was added. The mixture was stirred and refluxed at 70 °C for 3 h and then 8.6 mL of TEOS was added dropwise. After stirring for an additional hour, the resultant milky white solution was transferred into an autoclave and heated at 90 °C for 24 h. After the hydrothermal treatment, the autoclave was cooled to room temperature. The solid was recovered by filtration, washed with distilled water, and dried at 60 °C. Afterwards, the template was removed by calcination at 560 °C for 6 h. The silica samples prepared in such a manner were designated as Sn, with n indicating the length of alkyl chain of the C_nTMABr template.

2.2. Synthesis of amine-functionalized mesoporous silicas

Amine-functionalized mesoporous silicas were prepared according to the procedure reported before [29]. In our experiments, the organoalkoxysilanes containing one, two and three amino groups, namely (3-aminopropyl)triethoxysilane ($C_9H_{23}NO_3Si$), *N*-[3-(trimethoxysilyl)propyl]ethylenediamine ($C_8H_{22}N_2O_3Si$), and N^1-(3-trimethoxysilylpropyl)diethylenetriamine ($C_{10}H_{27}N_3O_3Si$), were supplied by Aldrich Chemicals and were selected for the functionalization process. It is expected that different densities of amino groups would be grafted on the prepared silica samples. In a typical synthesis, 0.6 g of as-prepared mesoporous silicas was dispersed in 60 mL of dry toluene and then 3 mL of organoalkoxysilane precursor was added; the mixture was refluxed under a nitrogen atmosphere for 12 h. The powder was collected by filtration, washed with isopropanol, and dried at 80 °C in dry nitrogen for 12 h. The amine-grafted silica materials were denoted as mesoporous silica-1N, -2N, and -3N corresponding to organic chains containing one, two and three amino functional groups, respectively.

2.3. Characterization

Small-angle X-ray scattering (SAXS) measurements have been carried out with a rotating anode source with a Cu target. The beam size at the sample was approximately 1 mm in diameter, and the scattering was recorded with a Princeton two-dimensional CCD camera located about 30 cm from the sample. For scanning electron microscopy (SEM) characterization of SiO_2, samples were dispersed onto 10 mm diameter aluminum specimen supports with conductive copper tape and colloidal graphite. Samples were coated with ca. 10 nm of gold using a Hummer 6.2 sputtering unit (Anatech Ltd., Hayward, CA) and examined using a JEOL JSM-5600 SEM (JEOL USA, Peabody, MA). Images were collected using an accelerating voltage of 10 kV at a working distance of 8 mm. Transmission electron microscopy (TEM) of the nanoporous SiO_2 was preformed by placing a small amount of sample into a glass vial. Ethanol was added and the solution was sonicated for 10 min. A drop of the solution was placed onto a carbon-coated, 200 mesh copper grid and left to dry overnight. The sample was imaged using a 2011 JEOL STEM at 200 keV. Images were captured with a 4k × 4k multiscan CCD camera using Digital Micrograph from Gatan. Fourier transform infrared (FTIR) spectra of the samples were collected with a LabRam-IR HR800 system from HORIBA Jobin Yvon Co. This system consisted of a combination of a miniaturized IlluminatIR-interferometer from SensIR Technologies, Ltd. and a high-resolution dispersive Raman spectrometer equipped with a confocal Olympus microscope. An all reflecting objective was used for collecting FTIR spectra of samples. Spectra acquisition and data processing were done using QualID software with 64 scans at a 4 cm^{-1} resolution. Nitrogen (N_2) adsorption–desorption isotherms were collected at 77 K using Micromeritics Tri-Star II 3020 equipment. All SiO_2 samples were degassed at 80 °C for 12 h prior to measurements. The specific surface area (S_{BET}) was determined by the multipoint Brunauer–Emmett–Teller (BET) method using the adsorption data in relative pressure (P/P_0) range of 0.05–0.2. The total pore vol-

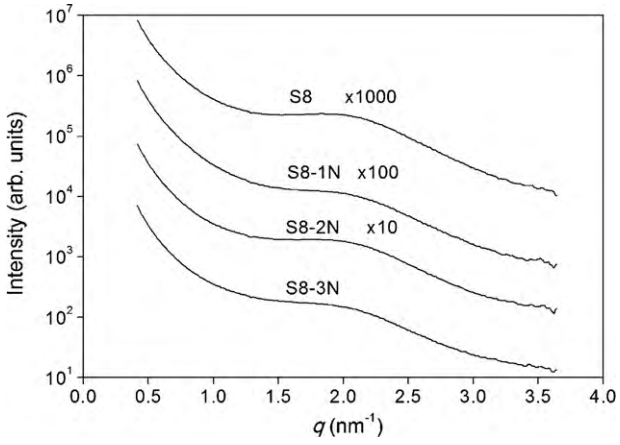

Fig. 1. SAXS patterns of silica S8 and its functionalized derivatives on a semilogarithmic scale as a function of the scattering vector q. The curves are shifted vertically by multiplication with the indicated factors.

ume (V_t) and average pore size (D_A) were determined by the nitrogen adsorption volume at the relative pressure of 0.99. The pore size distribution was determined by the desorption branch of the isotherm using the Barret–Joyner–Halender (BJH) method. The nitrogen (N) content was determined by elemental microanalysis on an Elementar Vario-Macro analyzer of Elementar Analysensysteme GmbH.

2.4. Heavy metal adsorption experiments

Before the adsorption experiments, all glassware was washed with concentrated hydrochloric acid, concentrated nitric acid and deionized water. In order to test the heavy metal removal ability of the as-prepared materials, a series of adsorption experiments were carried out by stirring 50 mg of silica powder in 25 mL of a heavy metal solution at 25 °C. The aqueous systems selected were arsenic (III), cadmium (II), lead (II), iron (III) and manganese (II). The starting metal salts used were nitrates (purity 99.999%) in all cases except for arsenic oxide (purity 99.995%). Initial concentration of the aqueous solution for these experiments was around 0.5 mg/L (0.5 ppm). In order to prevent the precipitation of metallic cations [30], the initial solution pH was adjusted to about 4.0 in our study. The mixture of silica adsorbent and heavy metal solution was stirred for 30 min and then filtrated with a 0.45 μm syringe filter to collect the final solution. The concentration of heavy metals in the initial and final solutions was determined by inductively coupled plasma atomic emission spectroscopy (ICP-AES). The analyses were performed in a Varian Vista MPX spectrometer after calibration with stock solutions. We repeated the adsorption experiments and the data were expressed as the average value.

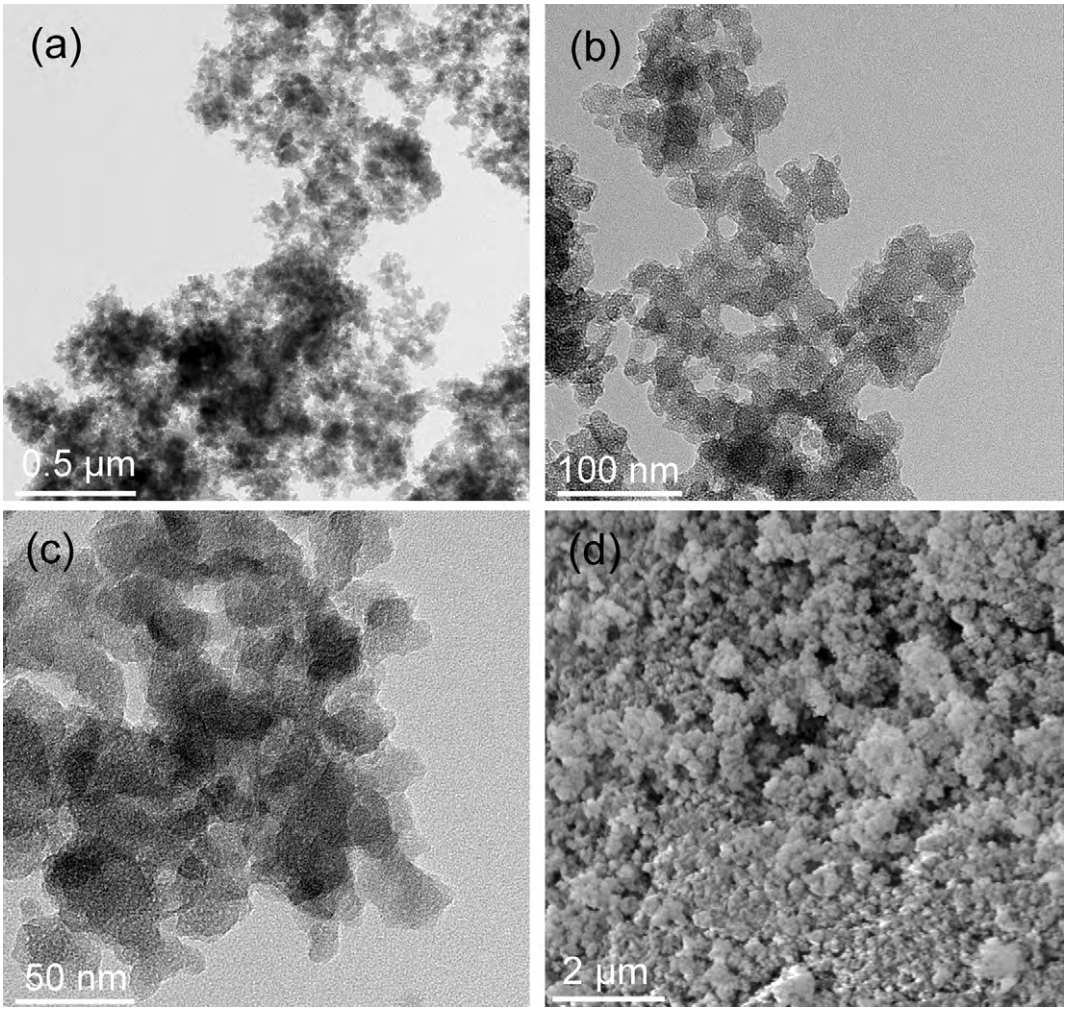

Fig. 2. TEM and SEM images of silica samples S8 (a, b, and d) and S8-1N (c).

3. Results and discussion

3.1. Structural and textural properties of silica S8 and the functionalized samples

The long-range order of the pores of the silica before and after grafting was characterized by SAXS measurements. Fig. 1 shows the SAXS patterns of silica S8 prepared using $C_8H_{17}(CH_3)_3NBr$ as template and its amine-functionalized samples. Strong scattering is observed below $q = 0.5\ nm^{-1}$, and a plateau or broad peak near $q = 2.0\ nm^{-1}$. This indicates a highly disordered structure with a typical pore size of 3 nm. The silica S8 and its functionalized samples were further investigated by TEM measurement, and the representative images are shown in Fig. 2. A hierarchical pore structure with small intra-particle pores and larger 10–100 nm inter-particle pores is revealed by the transmission electron micrograph in Fig. 2a and b. The SEM image of S8 in Fig. 2d shows that the porous silica has a loose, granular shape with the diameter of a few hundreds of nanometers. Upon grafting, the quantity of both small pores and larger pores decreases (Fig. 2c). This is probably because the grafted functional groups block some of the small pores.

Functional groups were identified using FTIR. Fig. 3 shows the FTIR spectra of the prepared samples between 1250 and 3750 cm^{-1}. For samples S8-1N, S8-2N and S8-3N (Fig. 3a), the broad NH_2 stretching vibration at 3250–3450 cm^{-1} and NH_3^+ deformation peak at 1540–1580 cm^{-1} are evident [13], confirming that the amino groups have been grafted successfully onto the pore surfaces of S8.

Fig. 4 shows the nitrogen adsorption–desorption isotherms and the corresponding pore size distributions calculated by the BJH method for silica S8 and the amine-functionalized samples. Textural properties obtained from the sorption data and the nitrogen contents of these hybrid samples are summarized in Table 1. Following the IUPAC classification, sample S8 exhibits a combination of type I and type II isotherm, and pore size distribution curve (Fig. 4b) indicating the presence of small pores of around 3 nm and larger pores of 10–100 nm. This corresponds well to the SAXS and TEM results (Figs. 1 and 2b). The specific surface area and pore volume of sample S8 are 548 m^2/g and 0.72 cm^3/g, respectively. After grafting, the nitrogen contents of S8-1N, S8-2N, and S8-3N are 2.53, 6.00, and 8.25 wt.%, respectively. The surface density of the functionalized groups depends on the amino ligands. For the

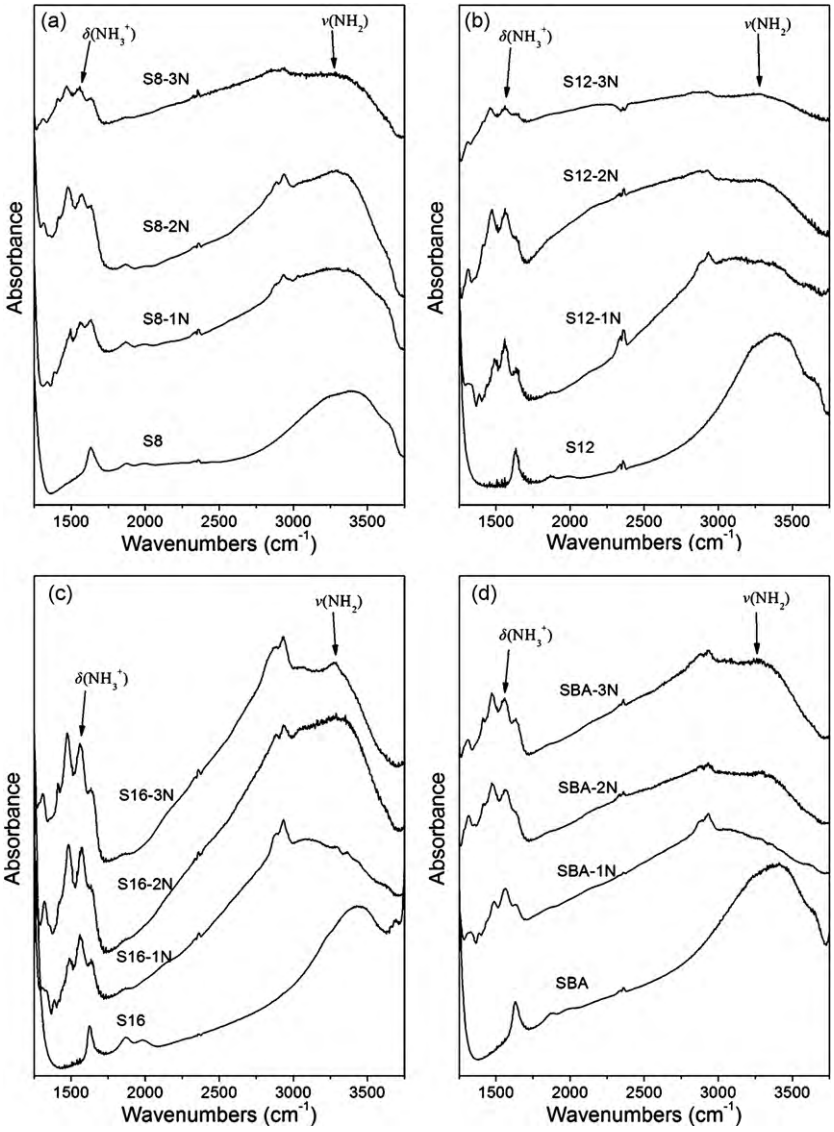

Fig. 3. FTIR spectra for unmodified silica samples S8 (a), S12 (b), S16 (c) and SBA (d) and their functionalized samples.

modified samples, the isotherms show type II characteristic of a type H3 hysteresis loop in the relative pressure range of 0.9–1.0. It can be seen that the N_2 adsorption arising from filling of small pores decreased remarkably in the P/P_0 range of 0–0.2. This indicates that the micropores and small mesopores were more easily filled with amino groups, restricting the access of nitrogen into the pores at the liquid nitrogen temperature. With the increase of surface density of functionalized groups, the specific surface area and pore volume were decreased to 77 m^2/g and 0.34 cm^3/g in S8-1N, 34 m^2/g and 0.25 cm^3/g in S8-2N, and 27 m^2/g and 0.15 cm^3/g in S8-3N, respectively.

3.2. Structural and textural properties of silica S12 and the functionalized samples

Fig. 5 shows the SAXS patterns of silica S12 and its amine-functionalized samples. An obvious peak with a maximum located at scattering vector (q) of 1.96 nm^{-1} was observed, with an intensity that is about four times higher that of the S8 sample, suggesting a more pronounced and better defined porous structure. The diffraction peak corresponds to a d-spacing (d_{100}) of 3.2 nm in the hexagonal system [25,26]. For the amino-functionalized samples, the presence of the diffraction peak indicates that all samples preserve the ordering of pore array after grafting. The reflection intensities are related to the degree of pore filling and the scattering contrast between the pore walls and the inside of the pores [31]. Hence, the decrease of SAXS intensity indicates a loss of scattering contrast, caused by the incorporation of organic chains containing amino groups into the pore channels of S12 [11,22,32,33]. The long-range periodicity of the microporous structure in sample S12 as indicated by SAXS was further supported by the TEM image (Fig. 6a). However, the electron microscopy picture of sample S12-1N (Fig. 6b) does not show a distinct porous structure. This is probably due to the occupation of the micropore channels by organic chains. The existence of functional groups in samples S12-1N, S12-2N and S12-3N can be proved by the FTIR spectra (Fig. 3b).

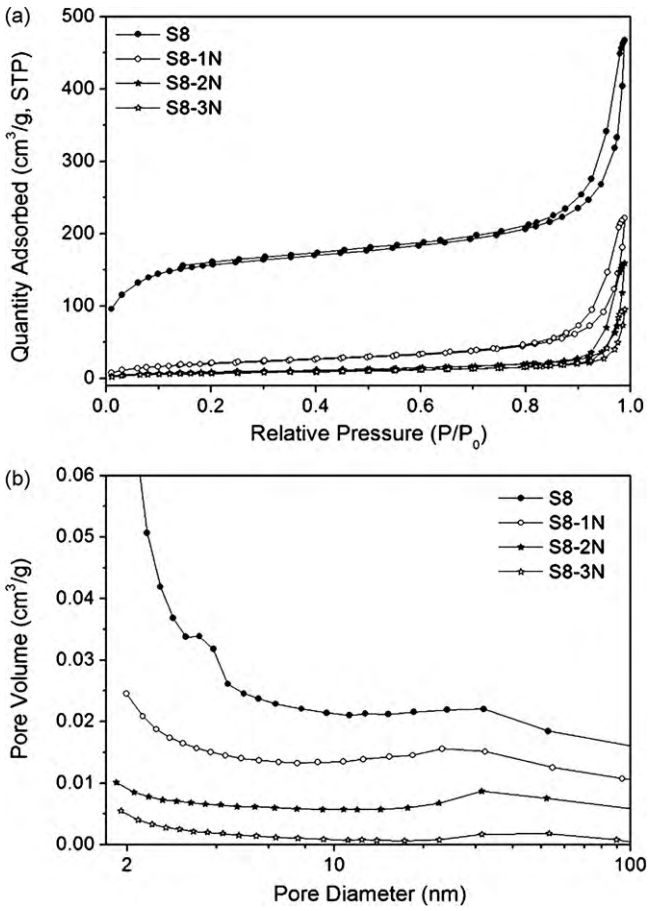

Fig. 4. N_2 adsorption–desorption isotherms at 77 K (a) and pore size distributions (b) of silica S8 and its functionalized samples.

Fig. 7 shows the nitrogen adsorption–desorption isotherms and the corresponding pore size distributions for silica S12 and the amine-functionalized samples. The isotherm of S12 is of type IV in the IUPAC classification with an adsorption step in the relative pressure range of 0.1–0.25. Although the pore volume of sample S12 is only 0.59 cm^3/g, it has a very high BET surface area of 1168 m^2/g. It is attributed to its microporous structure, which can be confirmed by the pore size distribution of S12 (Fig. 7b). As shown in Table 1, the N contents of S12-1N, S12-2N, and S12-3N are 4.66, 9.96, and 11.34 wt.%, respectively. It indicates that the high specific surface area is favorable to surface functionalization and thus enhance the ratio of amino groups. However, the amine-functionalized samples exhibit non-porous structures as shown by their isotherms and pore size distribution curves. This is probably because the organic

Table 1
Textural properties and nitrogen (N) content of the silica samples.

Samples	S_{BET}[a] (m^2/g)	V_t[b] (cm^3/g)	D_A[c] (nm)	D_{BJH}[d] (nm)	Nitrogen (N) content (wt.%)
S8	548	0.72	5.3	<2, 31.9	–
S8-1N	77	0.34	17.8	<2, 23.2	2.53
S8-2N	34	0.25	29.2	<2, 31.5	6.00
S8-3N	27	0.15	21.5	<2, 53.1	8.25
S12	1168	0.59	2.0	<2	–
S12-1N	8	0.02	8.0	–	4.66
S12-2N	1	0.002	6.2	–	9.96
S12-3N	1	0.002	6.0	–	11.34
S16	1064	0.94	3.5	2.7	–
S16-1N	728	0.34	1.9	<2	4.97
S16-2N	211	0.11	2.2	<2	7.03
S16-3N	6	0.01	7.6	–	9.82
SBA	877	1.16	5.3	6.5	–
SBA-1N	247	0.44	7.2	5.3	5.70
SBA-2N	26	0.07	11.1	5.4	8.90
SBA-3N	24	0.07	10.8	–	9.21

[a] BET surface area.
[b] Total pore volume.
[c] Average pore size.
[d] Pore size at peak maximum of the pore size distribution, determined by the BJH method.

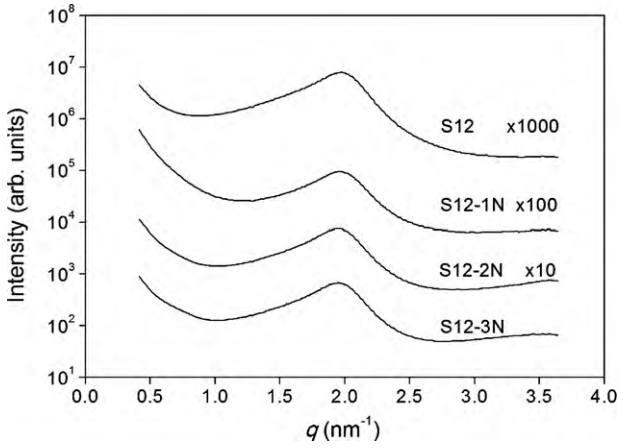

Fig. 5. SAXS patterns of silica S12 and its functionalized derivatives on a semilogarithmic scale as a function of the scattering vector q. The curves are shifted vertically by multiplication with the indicated factors.

groups can easily fill the uniform micropores and thus restrict the access of nitrogen into the pores.

3.3. Structural and textural properties of silica S16 and the functionalized samples

Fig. 8 shows the SAXS patterns of silica S16 and its amine-functionalized samples. A dominant peak at $q = 1.71\ nm^{-1}$ appears in the patterns of S16. The peak height is by about a factor two higher for S16 than for S12. The diffraction peak corresponds to a d-spacing of 3.7 nm, again in close agreement with the pore size found by nitrogen absorption (discussed below). The SAXS patterns of amino-functionalized samples show the same peak, which indicates that the pore structure was maintained during grafting. The decrease in the intensity of reflection is attributed to the occupation of pore channels. SEM measurement was used to assess the particle size, particle morphology, and the particle size distribution of the synthesized silica materials (Fig. 9a and b). Most particles of sample S16 are perfect spheres with a radius of 300–800 nm. For the amine-functionalized sample S16-3N, the spherical shape is maintained although some agglomeration is visible. The representative TEM images are shown in Fig. 9c and d. Two spherical S16 particles can be seen in the micrograph in Fig. 9c. The pore structure is regular over the whole particle, but as can be expected from the SAXS

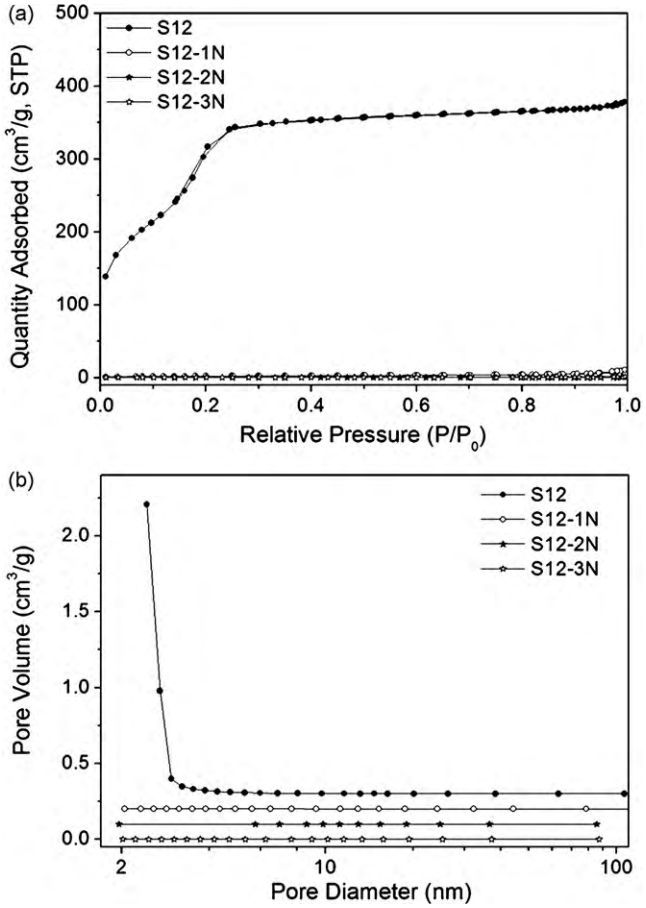

Fig. 7. N_2 adsorption–desorption isotherms (a) and pore size distributions (b) of silica S12 and its functionalized samples.

result, sample S16 does not possess the well-ordered hexagonal pore structure of MCM-41 materials synthesized in the absence of ethanol. After grafting, the spherical shape was preserved but the overall porosity decline could be observed (Fig. 9d). This is because the uniform small mesopores were partly occupied by the grafted organic groups.

As shown in Fig. 10a, the isotherm of sample S16 shows a typical type IV with a distinct adsorption step in the relative pressure range

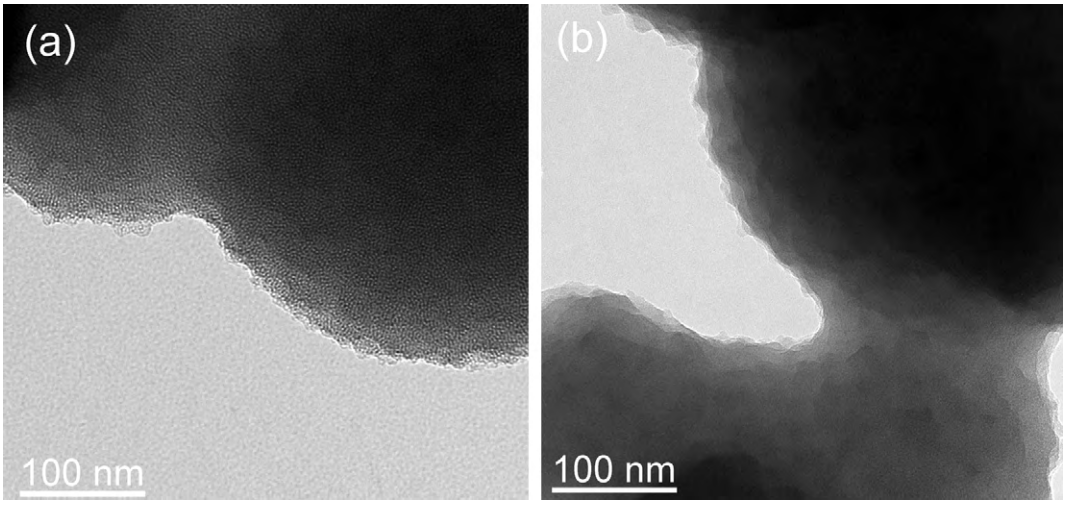

Fig. 6. TEM images of silica samples S12 (a) and S12-1N (b).

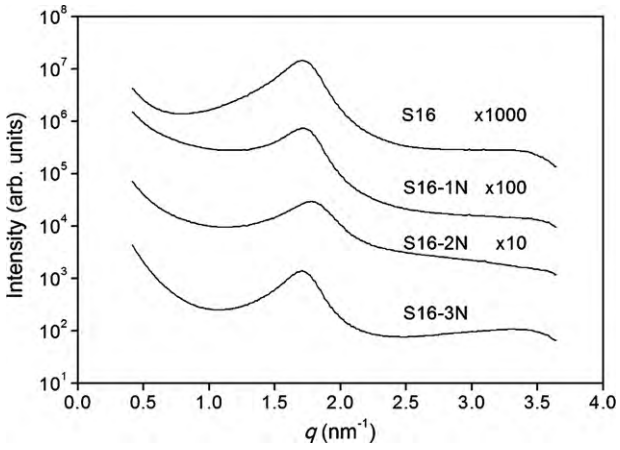

Fig. 8. SAXS patterns of silica S16 and its functionalized derivatives on a semilogarithmic scale as a function of the scattering vector q. The curves are shifted vertically by multiplication with the indicated factors.

of 0.25–0.35. The specific surface area, total pore volume and average pore size of silica S16 are 1064 m^2/g, 0.94 cm^3/g and 3.5 nm, respectively. In summary, the properties of the as-prepared silica materials S12 and S16 are similar as those of the spherical MCM-41 materials synthesized by well-established methods [25,26]. After grafting, the isotherms of S16-1N and S16-2N show the type I characteristic of microporous materials. It indicates the decrease of the pore size, which is also reflected in the pore size distributions (Fig. 10b). The peak maximum of the BJH pore size distributions decreased from 2.7 nm in S16 to less than 2 nm in S16-1N and S16-2N. The specific surface area and pore volume gradually decreased to 728 m^2/g and 0.34 cm^3/g in S16-1N, 211 m^2/g and 0.11 cm^3/g in S16-2N, and 6 m^2/g and 0.01 cm^3/g in S16-3N, respectively. The functional groups can be identified using FTIR (Fig. 3c). As shown in Table 1, the N contents of S16-1N, S16-2N, and S16-3N are 4.97, 7.03, and 9.82 wt.%, respectively.

3.4. Structural and textural properties of silica SBA and the functionalized samples

The FTIR spectra (Fig. 3d) and nitrogen contents (Table 1) of SBA as well as functionalized samples clearly indicate that the amino groups were grafted in the pores of SBA. Fig. 11 shows the SAXS patterns of silica SBA and its amine-functionalized derivatives. Seven well-resolved peaks can be indexed with *P6mm* hexagonal symmetry as shown in the diagram. For SBA the cell parameter is 11.1 nm. The diffraction patterns of SBA do not change much upon grafting with amino groups, which indicates that the ordered structure of the SBA is preserved. Compared with SBA, the (1 0 0) peaks shift to lower q values. The calculated unit cell parameter is 12.1 nm for SBA-1N, 11.6 nm for SBA-2N, and 11.3 nm for SBA-3N, implying the enlargement of the frameworks [34]. The decrease in the intensity of the diffraction peaks was observed in the amino-functionalized samples, again because the pores are filled with the organic molecules. The long-range periodicity of the porous structure as indicated by SAXS is supported by TEM results. A well-ordered mesoporous structure of hexagonal symmetry can be seen in the micrographs. The pore-to-pore distances match the SAXS

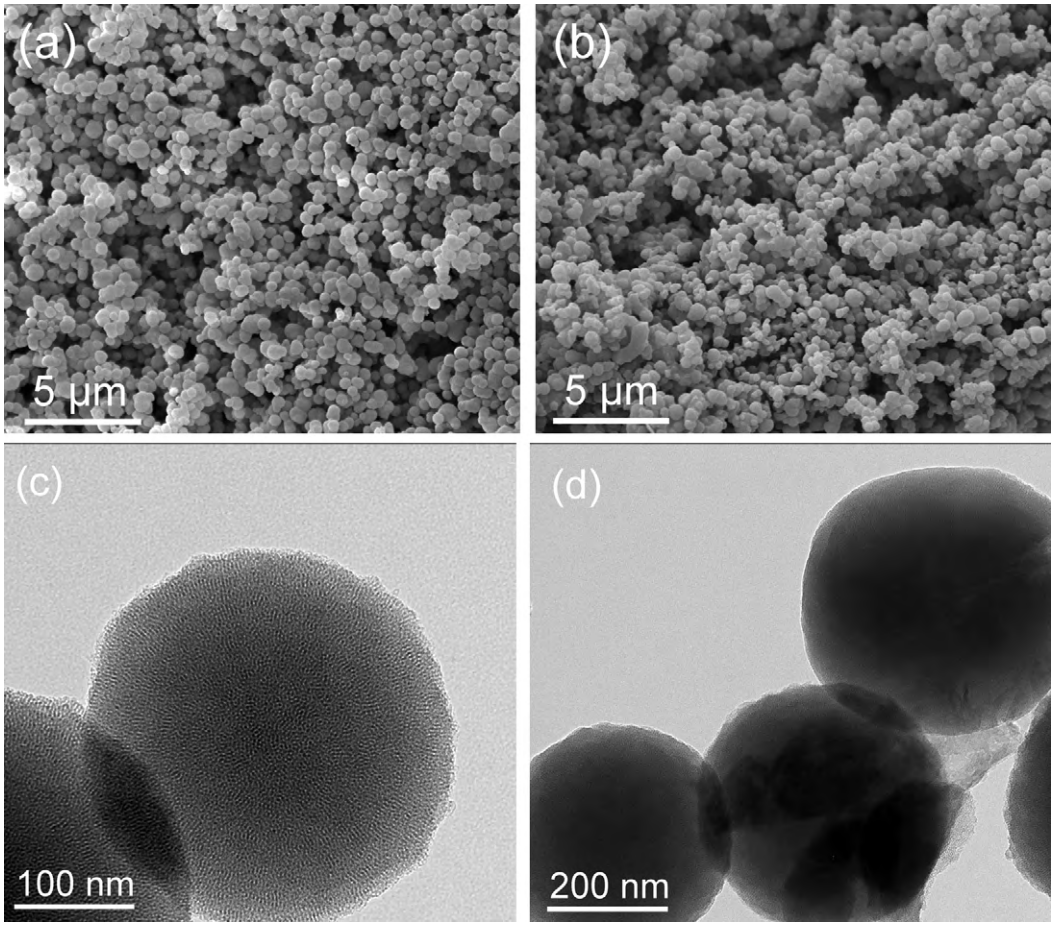

Fig. 9. SEM images of silica samples S16 (a) and S16-3N (b), and TEM images of samples S16 (c) and S16-1N (d).

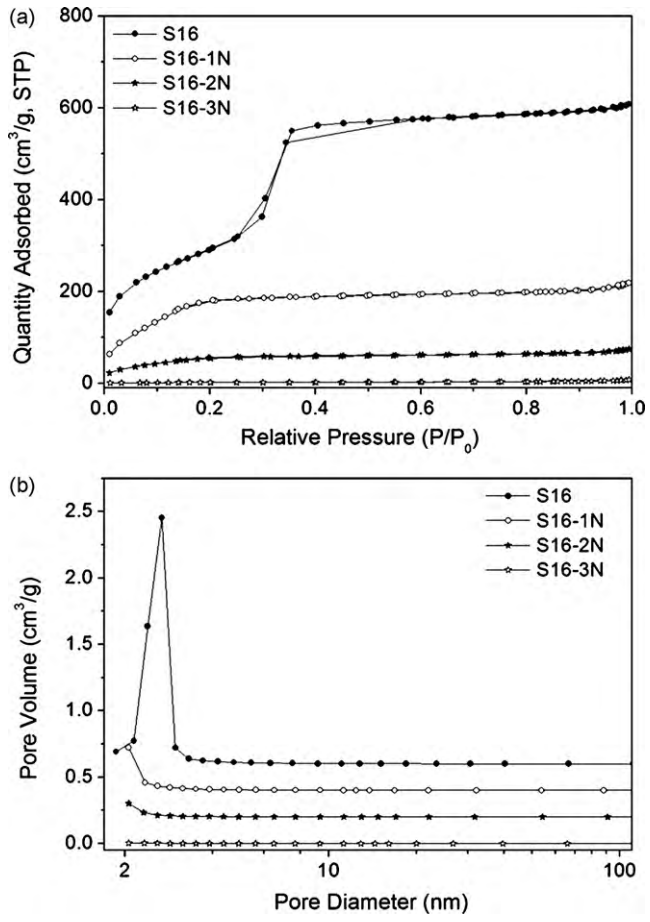

Fig. 10. N_2 adsorption–desorption isotherms (a) and pore size distributions (b) of silica S16 and its functionalized samples.

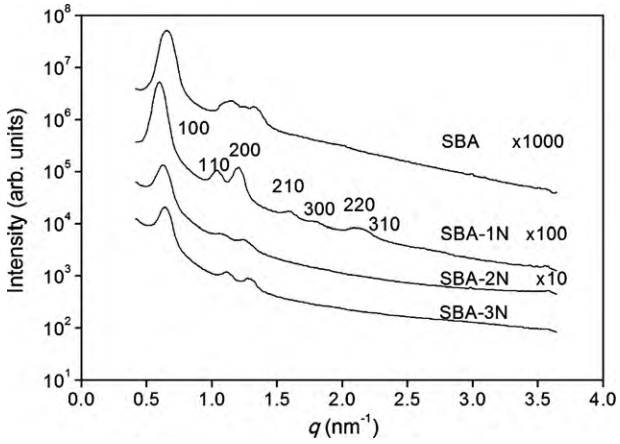

Fig. 11. SAXS patterns of silica SBA and its functionalized derivatives on a semilogarithmic scale as a function of the scattering vector q (points). The curves are shifted vertically by multiplication with the indicated factors. Peak indexing corresponds to a hexagonal lattice of pores.

results, with an increased lattice constant for SBA-1N relative to SBA. The mean pore size is about 7 (Fig. 12a). The TEM image for sample SBA-1N (Fig. 12b) confirms the existence of hexagonal structure viewed along the pore channels.

N_2 adsorption–desorption isotherms and the BJH desorption pore size distributions of SBA and its amine-grafted derivatives are shown in Fig. 13. Characteristic mesoporous type IV isotherms have been found for samples SBA and SBA-1N (Fig. 13a). Consistent with the decrease of nitrogen adsorption volume, the BET surface area and pore volume decreased from 877 m^2/g and 1.16 cm^3/g in SBA to 247 m^2/g and 0.44 cm^3/g in S16-1N, respectively. This is because the pore channels of SBA were partly filled with the organic molecules after grafting. Upon increasing the surface density of amino groups, only small surface areas and pore volumes were found in samples SBA-2N and SBA-3N. As the size of the grafted organic molecules in SBA-1N is much smaller than the pore diameter of 6.5 nm in SBA, minor change of the pore size was found between them. The peak pore diameters calculated by BJH method decrease from 6.5 nm for SBA to 5.3 nm for SBA-1N (Fig. 13b), which is in good agreement with the TEM results.

3.5. Heavy metal adsorption

Heavy metals such as As, Cd, Pb are common hazardous contaminants in drinking water supplies. These metals are potent carcinogenics and mutagenics. Although Fe and Mn are nontoxic metals and do not constitute a threat to human health, their presence in drinking water above a certain level causes aesthetic and operational problems such as odor, brown coloration, staining, turbidity and deposition in the water distribution systems [35,36]. According to the Guidelines for Canadian Drinking Water Quality [37], the maximum acceptable concentrations (MACs) for As(III), Cd(II), Pb(II), Fe(III), and Mn(II) are 0.01, 0.005, 0.01, 0.3, and 0.05 ppm (mg/L), respectively. Actually, unpublished data show that the concentrations of metals in some local drinking water are higher than the MACs. Therefore, simulated solutions containing

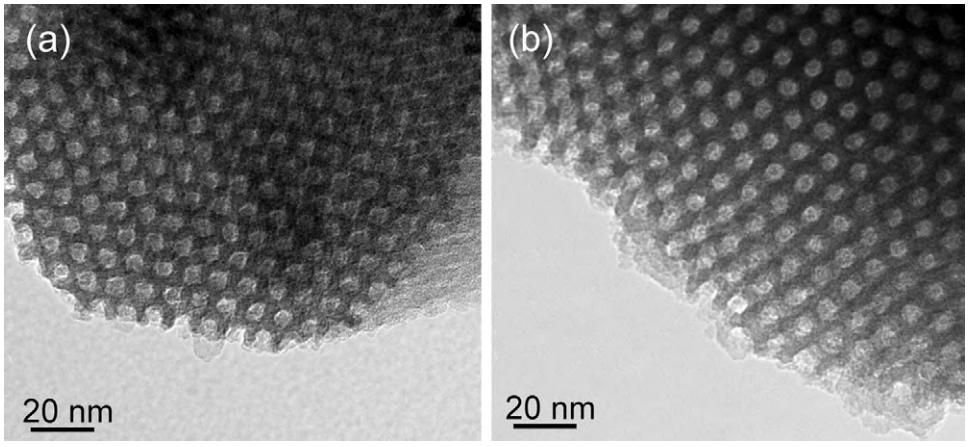

Fig. 12. TEM images of silica samples SBA (a) and SBA-1N (b).

approximate 0.5 ppm of heavy metals (As(III), Cd(II), Pb(II), Fe(III), or Mn(II)) were prepared in our experiments. Then series of adsorption experiments were carried out to test the ability of synthesized materials to act as heavy metal adsorbents.

Table 2 shows the concentrations of heavy metal ions in the simulated drinking water solutions before and after treatment with these adsorbents. The concentrations of metal ions were reduced to certain degrees after being treated with adsorbents for all kinds of metal ions with the exception of arsenic. In all samples no obvious adsorption was observed for arsenic. It is generally reported that As(III) does not have high affinity to the surface of various adsorbents compared with As(V) because As(III) exists mainly as nonionic H_3AsO_3 in natural water [38,39]. Thus, the removal of As(III) remains a challenge and a pretreatment of As(III) by oxidizing it to As(V) is necessary for its effective removal from water. As we can see from the results of our adsorption experiments, the adsorbents without grafting of amino groups show some adsorption of cadmium, lead, and iron cations. It indicates that the adsorption occurs even on the silanol groups of the silica surface. Significantly, the unmodified silica adsorbents can remove the Fe(III) cations almost completely from the simulated drinking water solutions. This is because the surface silanol groups have an affinity for Fe(III) and thus form a coordination complex [40]. As our experiments were performed at a pH value of about 4.0, it is likely the dominate Fe(III) species adsorbed occurred as $Fe(OH)_2^+$ according to the calculated equilibrium concentrations from Benjamin [41]. Accordingly, the dominate Cd(II) and Pb(II) species in our study should be Cd^{2+} and Pb^{2+}, respectively. The removal of Cd^{2+} and Pb^{2+} by the modified silica samples is attributed to the presence of active amino groups anchored to the porous silica walls. It was reported that the free amino groups could react with Cd^{2+} or Pb^{2+} to form stable metal complexes, in which the metal ions are coordinated by ligating N atoms of aminosilanes [7,22].

All hybrid silicas grafted with monoamino ligands (1N), with the exception of S12-1N, can effectively remove Cd(II), Pb(II), and Fe(III) completely. The removal of Mn(II) was also investigated and we found that the concentration of manganese cations decreased from 0.5136 mg/L of initial solution to below detective limit (0.0005 mg/L) of the final solution when using S16-1N as sorbent. The excellent performance of S16-1N can be ascribed to the accessibility of the functional groups in these adsorbents with high specific surface area and pore volume. Although silica S8-1N does not have high specific surface area, the large mesopores and macropores in S8-1N provide access to the amino groups. As shown in Table 2, 0.1311 mg/L of remaining Cd(II) was found in the solution after treatment with sample S12-1N. The small pore diameter of S12 is blocked upon grafting with amino groups, as indicated by the low surface area (8 m^2/g) and pore volume (0.02 cm^3/g) in S12-1N. Thus, steric hindrance limits the access of heavy metal ions to the binding sites deep inside the pores. The initial mass con-

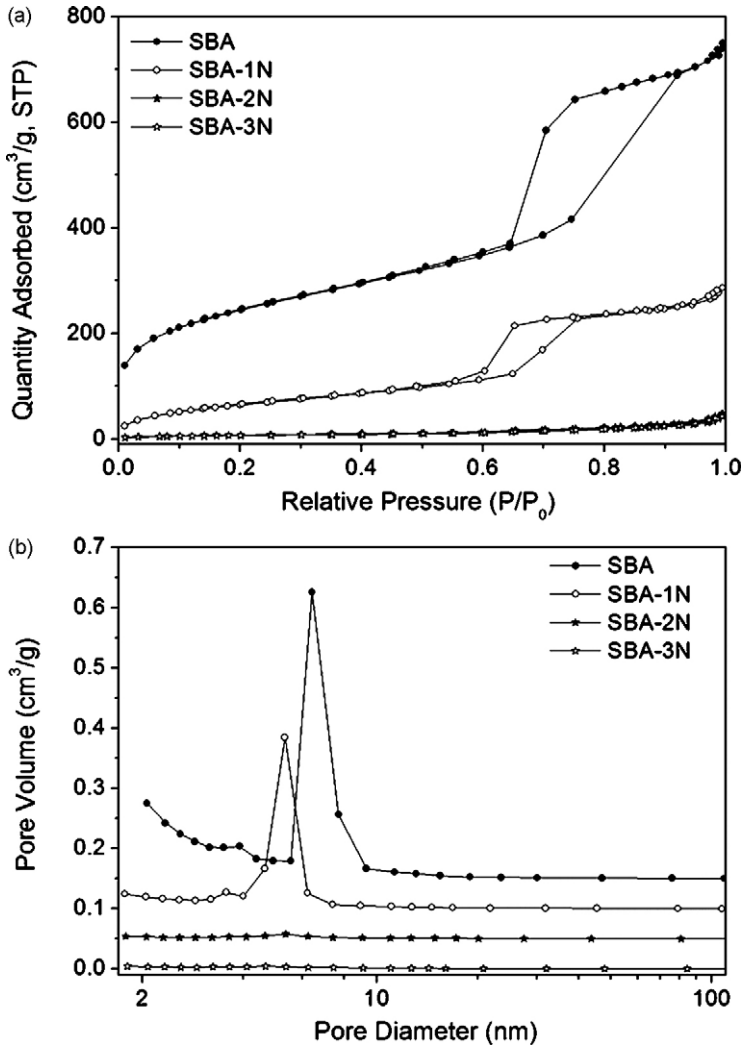

Fig. 13. N_2 adsorption–desorption isotherms (a) and pore size distributions (b) of silica SBA and its functionalized samples.

Table 2
The concentrations of heavy metal ions in simulated solutions before and after treatment with the prepared hybrid silica adsorbents.

Adsorbent	As(III) (mg/L)	Cd(II) (mg/L)	Pb(II) (mg/L)	Fe(III) (mg/L)	Mn(II) (mg/L)
No treatment	0.40	0.459	0.487	0.490	0.514
S8	0.41	0.328	0.266	0.007	0.437
S8-1N	0.49	<DL[a]	<DL[b]	<DL[c]	0.239
S8-2N	0.50	0.003	<DL	0.185	0.006
S8-3N	0.51	0.046	0.022	0.183	0.023
S12	0.39	0.375	0.293	0.002	0.451
S12-1N	0.44	0.131	<DL	<DL	0.399
S12-2N	0.50	0.055	0.062	0.391	0.220
S12-3N	0.49	0.191	0.287	0.442	0.294
S16	0.40	0.363	0.282	0.004	0.457
S16-1N	0.48	<DL	<DL	<DL	<DL[d]
S16-2N	0.48	<DL	<DL	<DL	0.330
S16-3N	0.49	0.003	0.045	0.337	0.270
SBA	0.41	0.387	0.079	0.003	NA[e]
SBA-1N	0.48	<DL	<DL	<DL	NA
SBA-2N	0.49	0.001	<DL	0.028	NA
SBA-3N	0.48	0.002	<DL	<DL	NA

[a] Detection limit for Cd(II) is 0.0008 mg/L.
[b] Detection limit for Pb(II) is 0.011 mg/L.
[c] Detection limit for Fe(III) is 0.002 mg/L.
[d] Detection limit for Mn(II) is 0.0005 mg/L.
[e] NA: data not available.

centrations were the same for all heavy metals, and initial molar concentration vary according to the atomic weight of each metal. Therefore, the initial molar concentration of Cd(II) is higher than that of Pb(II). As a result of treatment with S12-1N, the Pb(II) concentration was reduced below the detection limit, but only 71.5% of Cd(II) was removed.

To explore the effect of the type of amino groups, the results for adsorption of heavy metals based on diamino-grafted (2N) and triamino-grafted (3N) silica adsorbents are listed in Table 2. Generally, the heavy metal adsorption decreases with increasing N content for sample S8-2N, S8-3N, S12-2N, S12-3N, and S16-3N, indicating that the effectiveness of the amino groups decreases with the loading amount. Because the synthesized silicas have straight channel pores which are not interconnected, one of the likely reasons is more easily blockage by inhomogeneous grafted moiety (diamino and triamino ligands) with larger size near the pore mouths irrespective of the pore diameter of the silica. Moreover, high amino contents increase the probability of bottleneck formation at the pore entrances. It thus leads to the huge decrease of surface areas and pore volumes in the modified silicas, which can be confirmed from the textural properties of the grafted silica samples (Table 1). Such structure would lead to the rapid decrease in opportunities for the heavy metal ions to interact with effective amino groups located inside the pores. In addition, with the increase of the alkyl chain length and density of amino-organic moieties, the amino groups can more easily interact with adjacent amino groups by hydrogen bonding [42]. Depending on the relation between the pore diameter of the porous material and the size of the moiety to be grafted, steric hindrance can be different in the silica materials with tunable pore diameter. Because the larger pore diameter in S16 and SBA could provide access to sites deep inside the pores, their grafted silica adsorbents show superior performances. It can be seen that the treatment with sample S16-2N reduced the Cd(II), Pb(II), and Fe(III) concentration to below the detection limit. Although adsorbent SBA-3N exhibits really low specific surface area and pore volume, it could remove the heavy metal ions rather completely.

In our experiments, the best adsorbent was found to be S16-1N which could effectively remove heavy metal cations Cd(II), Pb(II), Fe(III), as well as Mn(II) from simulated drinking water. The outstanding property is closely related to the high specific surface area of 728 m^2/g, an open-pore structure with the total pore volume of 0.34 cm^3/g, and the accessibility of effective amino groups in S16-1N. Nevertheless, considering the low concentrations of heavy metals in the drinking water, further work is needed to determine the adsorption abilities of these adsorbents for heavy metal ions with much higher concentration. Another concern is the small particle size of the silica powder, which leads to difficulty in separating silica adsorbent from treated solution in application. Another route to obtain larger aggregates may be to mix the silica nanoparicles, either before or after functionalization, with polymer particles of suitable size and then to sinter the compressed mixture in the vicinity of the glass transition temperature of the polymer binder.

4. Conclusions

In the present work, hierarchical porous silica S8 and ordered hexagonal porous silica S12 and S16 were prepared by an uncommon surfactant-assisted templating method. For comparison, the well-known mesoporous silica SBA was also prepared. Based on these silica materials, amino-functionalized porous silica materials with tunable pore structures and morphology were synthesized by grafting of monoamino, diamino or triamino ligands. Structural characterization indicated that the hybrid materials exhibited varying degrees of decline of structure properties after functionalization, i.e. regular arrangement of pores, specific surface area, pore size, and pore volume, which depends on the relation between the pore diameter of the porous silica materials and the size and content of the moiety to be grafted. The hybrid silica materials are efficient adsorbents for the removal of heavy metal ions from drinking water. The abilities of the adsorbents were found to be closely related with the pore structure, pore density and the accessibility of the grafted amino groups. Monoamino-functionalized silica material S16-1N could completely remove Cd(II), Pb(II), Fe(III), and Mn(II), but not the nonionic As(III). The performance of S16-1N is similar to that in SBA-1N. We attribute the good performance to the accessibility of effective amino groups and suitable open-pore structure in S16-1N.

Acknowledgements

The financial support of the RTI of New Brunswick Innovation Fund (NBIF), and National Science and Engineering Research Council (NSERC) of Canada is gratefully acknowledged. R.Z. Ferguson

would like to thank NSERC for the Industrial Undergraduate Student Research Award, and the RAI of NBIF for the financial support. We would like to thank Fréderic de Geuser, SiMaP Grenoble, for his assistance with the SAXS measurements.

References

[1] R. Apak, E. Tütem, M. Hügül, J. Hizal, Heavy metal cation retention by unconventional sorbents (red muds and fly ashes), Water Res. 32 (1998) 430–440.
[2] D. Clifford, S. Subramonian, T.J. Sorg, Water treatment processes. III. Removing dissolved inorganic contaminants from water, Environ. Sci. Technol. 20 (1986) 1072–1080.
[3] S. Babel, T.A. Kurniawan, Low-cost adsorbents for heavy metals uptake from contaminated water: a review, J. Hazard. Mater. B 97 (2003) 219–243.
[4] K.S. Hui, C.Y.H. Chao, S.C. Kot, Removal of mixed heavy metal ions in wastewater by zeolite 4A and residual products from recycled coal fly ash, J. Hazard. Mater. 127 (2005) 89–101.
[5] A. Sayari, S. Hamoudi, Y. Yang, Applications of pore-expanded mesoporous silica. 1. Removal of heavy metal cations and organic pollutants from wastewater, Chem. Mater. 17 (2005) 212–216.
[6] J.P. Ruparelia, S.P. Duttagupta, A.K. Chatterjee, S. Mukherji, Potential of carbon nanomaterials for removal of heavy metals from water, Desalination 232 (2008) 145–156.
[7] A.N. Vasiliev, L.V. Golovko, V.V. Trachevsky, G.S. Hall, J.G. Khinast, Adsorption of heavy metal cations by organic ligands grafted on porous materials, Microporous Mesoporous Mater. 118 (2009) 251–257.
[8] X. Feng, G.E. Fryxell, L.Q. Wang, A.Y. Kim, J. Liu, K.M. Kemner, Functionalized monolayers on ordered mesoporous supports, Science 276 (1997) 923–926.
[9] L. Mercier, T.J. Pinnavaia, Access in mesoporous materials: advantages of a uniform pore structure in the design of a heavy metal ion adsorbent for environmental remediation, Adv. Mater. 9 (1997) 500–503.
[10] A.M. Liu, K. Hidajat, S. Kawi, D.Y. Zhao, A new class of hybrid mesoporous materials with functionalized organic monolayers for selective adsorption of heavy metal ions, Chem. Commun. (2000) 1145–1146.
[11] H. Yoshitake, T. Yokoi, T. Tatsumi, Adsorption of chromate and arsenate by amino-functionalized MCM-41 and SBA-1, Chem. Mater. 14 (2002) 4603–4610.
[12] N. Chiron, R. Guilet, E. Deydier, Adsorption of Cu(II) and Pb(II) onto a grafted silica: isotherms and kinetic models, Water Res. 37 (2003) 3079–3086.
[13] L. Bois, A. Bonhommé, A. Ribes, B. Pais, G. Raffin, F. Tessier, Functionalized silica for heavy metal ions adsorption, Colloids Surf. A: Physicochem. Eng. Aspects 221 (2003) 221–230.
[14] T. Yokoi, H. Yoshitake, T. Yamada, Y. Kubota, T. Tatsumi, Amino-functionalized mesoporous silica synthesized by an anionic surfactant templating route, J. Mater. Chem. 16 (2006) 1125–1135.
[15] K.F. Lam, K.L. Yeung, G. McKay, A rational approach in the design of selective mesoporous adsorbents, Langmuir 22 (2006) 9632–9641.
[16] D. Pérez-Quintanilla, I. del Hierro, M. Fajardo, I. Sierra, Mesoporous silica functionalized with 2-mercaptopyridine: synthesis, characterization and employment for Hg(II) adsorption, Microporous Mesoporous Mater. 89 (2006) 58–68.
[17] L.X. Zhang, C.C. Yu, W.R. Zhao, Z.L. Hua, H.R. Chen, L. Li, J.L. Shi, Preparation of multi-amine-grafted mesoporous silicas and their application to heavy metal ions adsorption, J. Non-Cryst. Solids 353 (2007) 4055–4061.
[18] X.M. Xue, F.T. Li, Removal of Cu(II) from aqueous solution by adsorption onto functionalized SBA-16 mesoporous silica, Microporous Mesoporous Mater. 116 (2008) 116–122.
[19] L.C. Cides da Silva, L.B.O. dos Santos, G. Abate, I.C. Cosentino, M.C.A. Fantini, J.C. Masini, J.R. Matos, Adsorption of Pb^{2+}, Cu^{2+} and Cd^{2+} in FDU-1 silica and FDU-1 silica modified with humic acid, Microporous Mesoporous Mater. 110 (2008) 250–259.
[20] R.K. Dey, C. Airoldi, Designed pendant chain covalently bonded to silica gel for cation removal, J. Hazard. Mater. 156 (2008) 95–101.
[21] C.A. Quirarte-Escalante, V. Soto, W. de la Cruz, G.R. Porras, R. Manríquez, S. Gomez-Salazar, Synthesis of hybrid adsorbents combining sol–gel processing and molecular imprinting applied to lead removal from aqueous streams, Chem. Mater. 21 (2009) 1439–1450.
[22] J. Aguado, J.M. Arsuaga, A. Arencibia, M. Lindo, V. Gascón, Aqueous heavy metals removal by adsorption on amine-functionalized mesoporous silica, J. Hazard. Mater. 163 (2009) 213–221.
[23] M. Arkas, D. Tsiourvas, Organic/inorganic hybrid nanospheres based on hyperbranched poly(ethylene imine) encapsulated into silica for the sorption of toxic metal ions and polycyclic aromatic hydrocarbons from water, J. Hazard. Mater. 170 (2009) 35–42.
[24] R.G. Peasron, Hard and soft acids and bases, J. Am. Chem. Soc. 85 (1963) 3533–3539.
[25] M. Grün, K.K. Unger, A. Matsumoto, K. Tsutsumi, Novel pathways for the preparation of mesoporous MCM-41 materials: control of porosity and morphology, Microporous Mesoporous Mater. 27 (1999) 207–216.
[26] M. Griin, I. Lauer, K.K. Unger, The synthesis of micrometer- and submicrometer-size spheres of ordered mesoporous oxide MCM-41, Adv. Mater. 9 (1997) 254–257.
[27] J.M. Rosenholm, M. Lindén, Wet-chemical analysis of surface concentration of accessible groups on different amino-functionalized mesoporous SBA-15 silicas, Chem. Mater. 19 (2007) 5023–5034.
[28] D. Zhao, J. Feng, Q. Huo, N. Melosh, G.H. Fredrickson, B.F. Chmelka, G.D. Stucky, Triblock copolymer syntheses of mesoporous silica with periodic 50 to 300 angstrom pores, Science 279 (1998) 548–552.
[29] W.H. Zhang, J.L. Shi, H.R. Chen, Z.L. Hua, D.S. Yan, Synthesis and characterization of nanosized ZnS confined in ordered mesoporous silica, Chem. Mater. 13 (2001) 648–654.
[30] Y.J. Jiang, Q.M. Gao, H.G. Yu, Y.R. Chen, F. Deng, Intensively competitive adsorption for heavy metal ions by PAMAM–SBA-15 and EDTA–PAMAM–SBA-15 inorganic–organic hybrid materials, Microporous Mesoporous Mater. 103 (2007) 316–324.
[31] M.B. Yue, L.B. Sun, Y. Cao, Y. Wang, Z.J. Wang, J.H. Zhu, Efficient CO_2 capturer derived from as-synthesized MCM-41 modified with amine, Chem. Eur. J. 14 (2008) 3442–3451.
[32] X.C. Xu, C.S. Song, J.M. Andresen, B.G. Miller, A.W. Scaroni, Novel polyethylenimine-modified mesoporous molecular sieve of MCM-41 type as high-capacity adsorbent for CO_2 capture, Energy Fuels 16 (2002) 1463–1469.
[33] V. Zeleňák, M. Badaničová, D. Halamová, J. Čejka, A. Zukal, N. Murafa, G. Goerigk, Amine-modified ordered mesoporous silica: effect of pore size on carbon dioxide capture, Chem. Eng. J. 144 (2008) 336–342.
[34] J. Zhu, Z. Kónya, V.F. Puntes, I. Kiricsi, C.X. Miao, J.W. Ager, A.P. Alivisatos, G.A. Somorjai, Encapsulation of metal (Au, Ag, Pt) nanoparticles into the mesoporous SBA-15 structure, Langmuir 19 (2003) 4396–4401.
[35] B. Das, P. Hazarika, G. Saikia, H. Kalita, D.C. Goswami, H.B. Das, S.N. Dube, R.K. Dutta, Removal of iron from groundwater by ash: a systematic study of a traditional method, J. Hazard. Mater. 41 (2007) 834–841.
[36] S.Y. Qin, F. Ma, P. Huang, J.X. Yang, Fe (II) and Mn (II) removal from drilled well water: a case study from a biological treatment unit in Harbin, Desalination 245 (2009) 183–193.
[37] Guidelines for Canadian Drinking Water Quality – Summary Table, 2008, available at: http://www.hc-sc.gc.ca/ewh-semt/pubs/water-eau/sum_guide-res_recom.
[38] Q. Li, N.J. Easter, J.K. Shang, As(III) removal by palladium-modified nitrogen-doped titanium oxide nanoparticle photocatalyst, Environ. Sci. Technol. 43 (2009) 1534–1539.
[39] J. Hao, M.J. Han, C. Wang, X. Meng, Enhanced removal of arsenite from water by a mesoporous hybrid material—thiol-functionalized silica coated activated alumina, Microporous Mesoporous Mater. 124 (2009) 1–7.
[40] A. Costine, S. Thurgate, Iron adsorption on SiO_2/Si(1 1 1), Surf. Interface Anal. 39 (2007) 711–714.
[41] M.M. Benjamin, Water Chemistry, McGraw-Hill, Boston, 2002.
[42] M.W. McKittrick, C.W. Jones, Toward single-site functional materials—preparation of amine-functionalized surfaces exhibiting site-isolated behavior, Chem. Mater. 15 (2003) 1132–1139.